

**Li<sup>+</sup>-ion neutralization on metal surfaces and thin films**Lin Chen,<sup>1,2</sup> Jie Shen,<sup>1</sup> Juanjuan Jia,<sup>1</sup> Thirunavukkarasu Kandasamy,<sup>1</sup> Kirill Bobrov,<sup>1</sup> Laurent Guillemot,<sup>1</sup> Javier. D. Fuhr,<sup>3</sup> Maria Luz Martiarena,<sup>3</sup> and Vladimir A. Esaulov<sup>1,\*</sup><sup>1</sup>*Institut des Sciences Moléculaires d'Orsay, (UMR8214, CNRS—Université Paris-Sud), F-91405 Orsay Cedex, France*<sup>2</sup>*School of Nuclear Science and Technology, Lanzhou University, Lanzhou 730000, China*<sup>3</sup>*Consejo Nacional de Investigaciones Científicas y Técnicas (CONICET) and Instituto Balseiro, Centro Atómico Bariloche, Bariloche, Rio Negro, Argentina*

(Received 15 June 2011; published 15 November 2011)

Li<sup>+</sup> ions with energies ranging from 0.3 to 2 keV are scattered from Au(110) and Pd(100) surfaces and from ultrathin Ag film grown on Au(111) in order to study electron transfer phenomena. We find that neutralization occurs quite efficiently and find an anomalous ion energy dependence of the neutral fraction for Au(110) and Pd(100) surfaces previously noted for Au(111). The dependence of the neutral fraction on the azimuthal angle of the Au(110) and Pd(100) surfaces is reported. In the case of Ag monolayer on Au(111), results are similar to the case of the Ag(111) surface. To understand the anomalous ion energy dependence, we present a theoretical study using density functional theory (DFT) and a linearized rate equation approach, which allows us to follow the Li charge state evolution for the (111) surfaces of Ag, Au, and Cu, and for the Ag-covered Au(111) surface.

DOI: [10.1103/PhysRevA.84.052901](https://doi.org/10.1103/PhysRevA.84.052901)

PACS number(s): 34.35.+a, 34.50.-s, 71.15.Mb

**I. INTRODUCTION**

Electron transfer processes on surfaces have been quite extensively investigated in the past, as they play an important role in surface chemistry and influence charge states of ions or atoms scattered on surfaces. Most of the experimental work has involved alkali-metal ion neutralization or negative ion formation in ion scattering experiments [1–15]. Recently renewed activity has developed in relation with some theoretical work, which points out that [16–22] energies and widths of atomic states for fixed atom-surface distance are strongly affected by the existence of band gaps and surface states. At the same time experimental and theoretical studies indicate that these effects, predicted for the case of static atoms, may not always be observable in the case of scattering experiments because of nonadiabatic effects in scattering with finite velocities [18,19,21,22]. Furthermore the role of *d* electrons and their influence on hybridization of Li *s-p* states and the Li(2*s*) lifetime in front of transition and noble metal surfaces has been discussed [16,23].

Recent developments in this field involve nanoscaled structures. Thus scattering on clusters and monolayer thin films has attracted attention [24–26]. Experimental studies of alkali-metal neutralization on supported Ag and Au clusters were performed [24,25] in the quest of observation of quantum-size effects [27–29], and showed that alkali-metal neutralization proceeds much more efficiently on small clusters than on films or bulk metal surfaces. Recent theory has also addressed the case of electron transfer on ultrathin films [30,31] and the effect of quantization because of the finite thickness of the film. Again it was concluded that under certain conditions electron transfer processes could be strongly affected.

The studies of alkali-metal ion neutralization on clusters and thin films [24,26] revealed a very curious feature, which is not understandable in “standard” models. Thus in the limit of complete surface coverage by Au(111)-type films

it was observed that efficient neutralization of Li occurs, in spite of a very large (5.4 eV) work function [32]. Usual chemisorption calculations [23,33] corresponding to fairly large distances (>5 a.u.) from the surface show that on metals the alkali-metal-projected density of states lies above the Fermi level. Similarly when one considers the “upward” image potential-induced shift of the Li(2*s*) level (ionization potential = 5.39 eV) to lower binding energies, which places it above the Fermi level, one can expect that electron capture will be very inefficient for surfaces with work functions of the order of 5 eV and higher. The result for the gold film was thus very surprising. In an endeavor to understand this feature we performed measurements of Li<sup>+</sup> neutralization on Cu(100), Cu(111), Au(111), and Au(100) surfaces [34,35]. These experiments revealed that, consistently, neutralization is “anomalously” large on these surfaces.

The existence of the *L* band gap for (111) surfaces was invoked [34] to allow for larger survival rates for neutralized Li; nonresonant charge exchange [36–40] involving surface states was considered. More recent theoretical work [41] has brought to light a key point in this context. The results of a calculation of the Li-Cu surface distance dependence of the Li level showed that the Li level at distances below 4 a.u. from the first atomic plane shifts again *below* the Fermi level: a shift attributable [41] to a balance between repulsive and attractive short-range interactions (electron-electron, nuclei-electrons). Thus in fact neutralization *can* occur for small ion-surface distances. This allowed [35,41] investigators to account for the existence of the hitherto unexpected neutralization, but the existing modeling remains incomplete and has been unable to reproduce the overall features of neutralization for these systems. This situation hinders further investigation into nanostructured systems, since understanding of the simpler case of bulk surfaces is an essential prerequisite.

In view of all these developments and as a concluding sequel to our earlier study of some noble metal surfaces, we decided to investigate Li<sup>+</sup> neutralization on Au(110), Pd(100), and Ag layers grown on Au(111). Our interest in Au(110) is due to

\*Corresponding author: [vladimir.esaulov@u-psud.fr](mailto:vladimir.esaulov@u-psud.fr)

two aspects: While Au(111) and Au(100) present a band gap at  $\bar{\Gamma}\bar{K}$  or  $\bar{\Gamma}\bar{X}$  directions in reciprocal space [32] which should impede electron loss for  $k_{\parallel}$  close to zero, this is not the case for Au(110). Also the Au(110) surface presents a  $(1 \times 2)$  missing row reconstruction, which could allow observation of trajectory-related effects that should help to shed additional light on the electron transfer dynamics. Our interest in Pd(100) is related to studies on Pd clusters on oxides, which are typical model catalyst systems [42]. A study of cluster-size effects on electron transfer for this case is interesting and planned. A prerequisite for this is the knowledge of the characteristic of neutralization on the bulk surface, hence this investigation. We also address the case of Ag layer grown on Au(111), where the electronic structure of the monolayer film should reflect the existence of the Au(111) band gap and as is well known, results in a strong shift in the energies of surface states [43]. We also present some scanning tunneling microscopy (STM) data on Ag growth on Au(111), which was performed to get insight into Ag overlayer growth.

The experiments are complemented by a theoretical study, using density functional theory (DFT) and a linearized rate equation approach, of the evolution of the Li charge in front of the (111) surfaces of Au, Ag, and Cu, and in front of a Ag monolayer on Au(111). Although the temporal evolution is taken into account only in a first approximation, the study of the static system from first principles helps us to understand, at least qualitatively, the characteristics of the system.

## II. EXPERIMENTAL SETUP

The ion scattering experiments were performed on an ultrahigh vacuum (UHV) system, described elsewhere [35]. This is equipped for ion scattering spectroscopy (ISS), time of flight (TOF) scattering, and recoiling spectroscopy (TOF-DRS), and a  $\text{Li}^+$  source, an  $\text{Ar}^+$  source for sputtering, and a third source used to produce other types of ions (H, O, F, etc.).

The STM experiments were carried out in a separate setup, equipped with a variable-temperature STM (Omicron VT-STM) using polycrystalline W tips. The STM chamber is coupled with a second one, where the usual devices for sample preparation as well as low-energy electron diffraction (LEED) and Auger electron spectroscopy (AES) measurements are available. A third small chamber is used as a load lock for samples and tips and also for in-vacuum tip preparation. The base pressure in the setup is of the order of  $5.0 \times 10^{-11}$  mbar.

On both setups the same Ag evaporator was used. For Ag evaporation we use a Ag wire wrapped around a tungsten filament. The evaporation was performed after the sample was cooled down to room temperature. The filament current of the evaporator was set at 4.6 A to maintain the deposition rate of  $0.2 \text{ \AA}/\text{min}$ . The amount of Ag deposited was monitored by a quartz crystal microbalance (QCM), ion scattering, and STM.

TOF measurements of energy losses of ions and neutrals and ion fraction measurements can be performed for forward or backward scattering measurements. The ion scattering system [38] is equipped with an ion and electron electrostatic analyzer and long flight tubes for ion and neutral TOF measurements. For Li backscattering we use a flight tube located at  $45^\circ$  from the Li gun, giving a  $135^\circ$  scattering angle (flight length 124 cm), while for forward scattering a tube located at  $97^\circ$  from

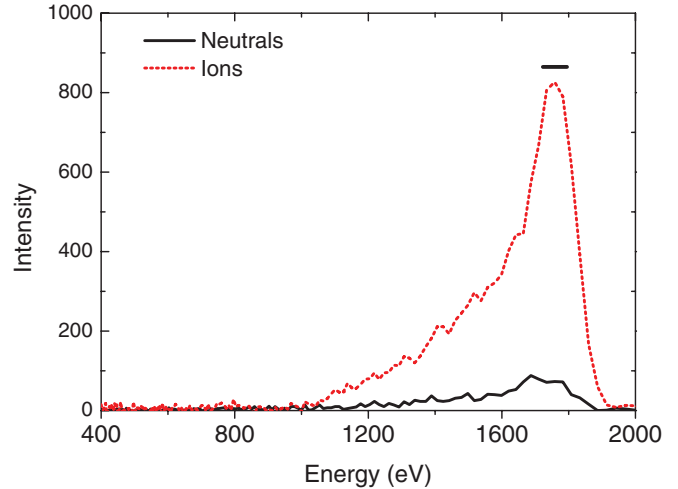


FIG. 1. (Color online) Energy spectra of 2-keV  $\text{Li}^+$  ions scattered off a Au(110) surface along a random crystal orientation, at a scattering angle of  $135^\circ$  under specular reflection. The horizontal bar indicates the integration region.

the  $\text{Li}^+$  source ( $83^\circ$  scattering angle; 198-cm flight length) is used. The tubes are equipped with multianode channel-plate detectors, allowing simultaneous separate detection of ions and neutrals in continuous- or pulsed-beam modes.

$\text{Li}^+$  ions are produced using a Li getter source.  $\text{Li}^+$  neutralization probabilities are determined by measuring neutral fractions for two scattering configurations corresponding to a total scattering angle of  $135^\circ$  and  $83^\circ$  and varying the incident (and hence exit) angle with respect to the surface. In the following, incident and exit angles are indicated with respect to the surface plane. The final “exit” energy of the backscattered Li projectile can be estimated simply from a classical binary collision model (BCM) considering scattering of Li mass  $M_1$  off a target atom of mass  $M_2$ , through a given scattering angle. Typical energy spectra are shown in Fig. 1 for 2-keV  $\text{Li}^+$  scattered from clean Au(110), after conversion of the time scale into an energy scale. One finds that they present a pronounced peak at higher energies corresponding to scattering from the topmost surface atoms. A broad lower-energy tail is related to inelastic energy losses resulting from particles penetrating into inner atomic layers or could also come from collision-induced reionization (recapture). Furthermore, the spectra for neutrals and ions are fairly similar.

The neutral fraction ( $\Phi^0$ ) is defined as the ratio of the number of  $\text{Li}^0$  and  $\text{Li}^0 + \text{Li}^+$  scattered into the detector [ $\Phi^0 = N(\text{Li}^0)/N(\text{Li}^0 + \text{Li}^+)$ ]. This can be measured in a continuous-beam mode or pulsed-beam mode using the TOF technique to analyze energy losses of scattered Li ions and atoms. In the latter case the neutral fractions can be extracted over a better-defined range of final energies by integrating over a finite range of the TOF energy spectrum indicated in Fig. 1 (horizontal bar). As previously studied on other surfaces in  $\text{Li}^+$  scattering, we did not observe significant differences between the neutral fractions measured by these two beam modes.

The crystals are cleaned as usual by multiple cycles of small-angle Ar bombardment and annealing. Cleanliness was checked by TOF-DRS, which is known to be sensitive to surface impurities (H, C, O, etc.) [44]. During sputtering, the

crystal was rotated azimuthally in order to avoid induction of structures due to sputtering. One of the main concerns in experiments of this type is the possibility of Li implantation which would change the surface work function. As in our previous studies and as mentioned above, we use a pulsed low-intensity ion beam which minimizes implantation. Furthermore cross checks of measured neutral fractions are made by changing the sequence of measurements in a given series, e.g., when changing incident energies and comparing data for the same conditions at the beginning and end of a series of measurements.

### III. THEORETICAL METHODS

We have carried out DFT calculations within the slab-supercell approach [45] by using the *ab initio* total energy and molecular dynamics program VASP (Vienna *ab initio* simulation program) [46,47]. The one-electron Kohn-Sham orbitals are developed using a plane-wave basis set, while electron-ion interactions are described through the projector augmented wave method [48]. Exchange and correlation (XC) is described within the generalized gradient approximation (GGA) introduced by Perdew, Burke, and Ernzerhof (PBE) [49]. The sampling of the Brillouin zone is carried out according to the Monkhorst-Pack method [50]. Electron smearing was introduced following the Methfessel-Paxton technique [51] with a width of the smearing equal to 0.2 eV and all the energies are extrapolated to 0 K. The employed energy cutoff is 350 eV. The theoretical lattice constant obtained for the Au, Ag, and Cu bulk (using a  $15 \times 15 \times 15$ -point mesh) is  $a_{\text{calc}} = 4.185 \text{ \AA}$ ,  $4.171 \text{ \AA}$ , and  $3.64 \text{ \AA}$ , respectively. We used a  $4 \times 4$  unit cell and four-layer slab to represent the metal (111) surface and  $3 \times 3 \times 1$   $k$ -point mesh. A vacuum layer of 24 layers ( $57.99 \text{ \AA}$  for Au,  $57.80 \text{ \AA}$  for Ag, and  $50.44 \text{ \AA}$  for Cu) in thickness was placed on top of the slab to ensure negligible interactions between periodic images normal to the surface. We represent the Ag monolayer on Au(111) substituting the Au topmost layer atoms by Ag atoms. Spin polarization is used for all the calculations.

We use the Bader method to calculate the charge around the Li atom [52]. The Bader analysis has been done considering the total charge density (core plus valence charge density). From now on, when we speak about Bader charge we are only referring to the number of lithium valence electrons.

### IV. Ag GROWTH ON Au(111)

The silver deposition was carried out with the Au(111) surface kept at room temperature to keep alloying effects weak even if little interdiffusion has been evidenced [53]. The surface was imaged after submonolayer deposition of Ag as shown in Fig. 2. In this figure white (or black) dotted lines show the gold sample terrace edges. Labels “M<sub>(n)</sub>” indicate the surface metal M and the level (n) of the terrace. Four different Au terrace levels are present showing the typical herringbone reconstruction going from the lowest one (1) at the bottom left corner to the highest one (4) at the top right corner. Ag islands are found on three of them. The typical topography of the grown islands confirms [54,55] the layer-by-layer growth mode of silver on Au(111) at room

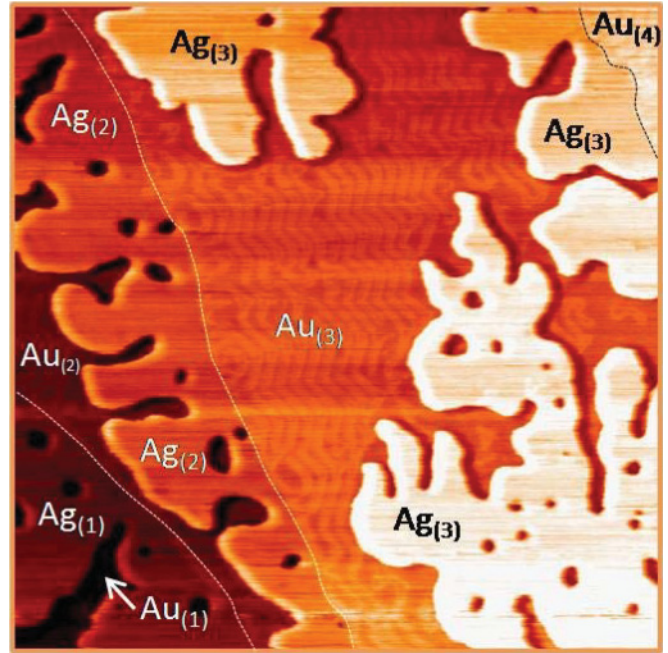


FIG. 2. (Color online) Constant current topographies of the Au(111) surface with  $\sim 0.6$  ML of Ag deposited at room temperature. The scale is  $320 \times 320 \text{ nm}^2$  [ $V_s = -0.6 \text{ V}$ ,  $I_t = 0.2 \text{ nA}$ ].

temperature. It can be further inferred that the silver layer growth starts at the interterrace steps of the gold sample.

On Fig. 3 the third-level Au(111) terrace (Au<sub>3</sub>) is readily seen with its characteristic herringbone reconstruction as well as the partial silver layer grown on the second-level gold terrace (Ag<sub>2</sub>). A clear distortion of the zigzag phase can be seen close to the terrace edge. The continuous ridge running along the Ag<sub>2</sub> layer as well as the U-shaped or looping ridges in the vicinity of the Ag<sub>2</sub> layer are typical of a {100} step [53]. On the silver layer a corrugation reminiscent of the Au reconstruction is visible. Nevertheless, one cannot say whether the underlying gold reconstruction is still present and shows through the silver layer or if the upper silver layer, itself, undergoes some reconstruction.

The height profile along the black line going through the Ag<sub>2</sub> and Au<sub>3</sub> interface shows a mean height difference between these two regions of  $65 \pm 10 \text{ pm}$ .

Then a higher coverage of Ag [ $\sim 2.4$  monolayers (ML)] was investigated and results are shown with four topographies at different scales in Fig. 4. Layer-by-layer growth mode is again observed. The second-layer Ag islands show peculiar fingerlike shapes and their growth also initiates at the silver-covered Au steps [Fig. 4(a)]. On the Ag layer a medium-scale corrugation manifests itself by the presence of some bright stripes reminiscent of the hexagonal close packed (hcp) ridges of the initial Au(111) reconstruction [Fig. 4(b)]. Figures 4(c) and 4(d) show a closeup on this particular region with atomic resolution. On this part of the terrace covered by two layers of Ag, the presence of ridges is clearly seen. One measures a distance between the two hcp ridges and also a corrugation very close to the one of the reconstructed Au(111) terraces. The atomic resolution of Fig. 4(d) clearly reveals a hexagonal unit mesh similar to Au(111) on most of the layer. Noteworthy

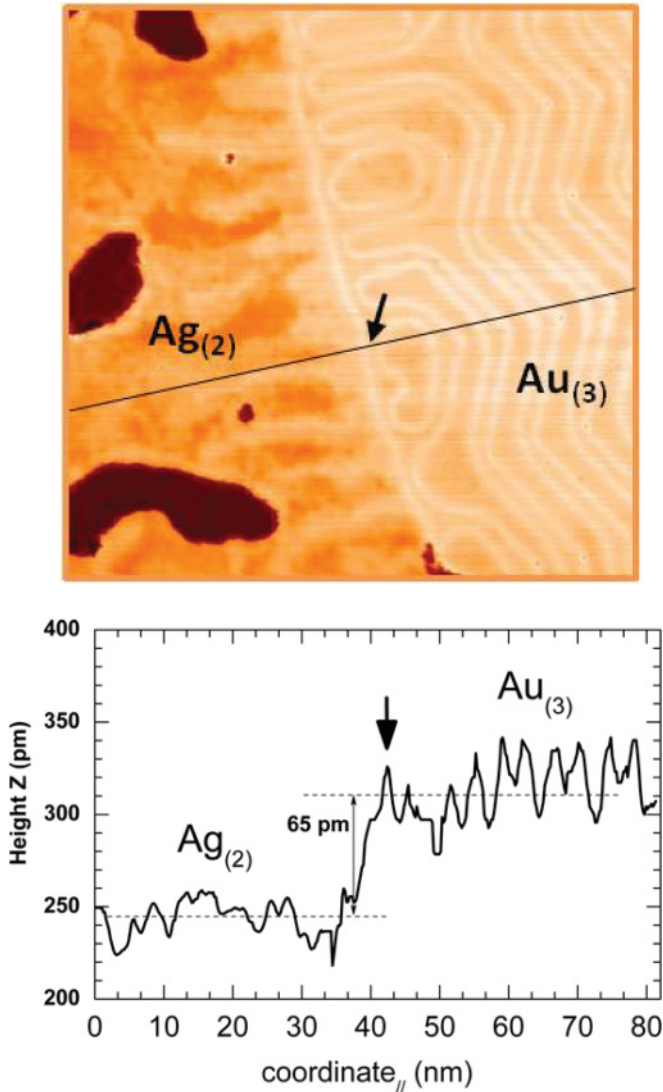


FIG. 3. (Color online) Constant current topography of the Ag/Au(111) interface. Upper panel: Closeup of Fig. 2, scaled  $80 \times 80 \text{ nm}^2$ , [ $V_s = -0.8 \text{ V}$ ,  $I_s = 0.2 \text{ nA}$ ]. Bottom panel: Height profile along the black line running through a silver-gold interface. The arrow is shown as a reference mark of the frontier between the Ag<sub>(2)</sub> and Au<sub>(3)</sub> regions.

is the inhomogeneous aspect of the outer layer at the atomic scale. Many atomic sites appear as black holes surrounded by six highlighted atoms, as can be seen in the inset of Fig. 4(d). This effect has already been reported and attributed to chemical contrast of different atomic species, obviously identified as gold atoms distributed in the silver layer [53]. This means that gold atoms diffuse from the substrate, intermixing with the silver layer. This was noticed in the case of a single Ag layer deposited on gold. Here we do identify the same gold atom intermixing effect for a double Ag layer. We were able to evaluate the number of gold inclusions as being  $5.9 \pm 0.2\%$  of the atomic sites of the layer. This value is close to the one consistent with the model proposed in [53]. Indeed this model assumes that the intermixing gold atoms could come from the lifting of the reconstruction at the Au(111) surface layer induced by the growth of the coating silver

layers. This would release 1/22 exceeding Au atoms of the herringbone structure, that is to say, close to 5% of the Au(111) surface atoms. Furthermore, to some extent we also find that the intermixing of gold atoms preferentially occurs in the pseudo-fcc regions. This would indicate that self-diffusion of gold atoms to the silver layer is region (fcc or hcp) dependent. Nevertheless, quasiabsence of gold atoms in the hcp regions (in between ridges marked by white dotted lines) finds a remarkable exception in the region marked by the white dotted oval.

## V. Li<sup>+</sup> NEUTRALIZATION

### A. Charge transfer processes of Li<sup>+</sup> scattering on a Au(110) surface

The definition of the azimuthal angles of the  $(1 \times 2)$  missing row reconstructed Au(110) surface is presented in Fig. 5(a). The range of azimuthal angles was chosen to include the three major crystallographic directions:  $[1\bar{1}0]$  surface channel at an azimuthal angle of  $0^\circ$ , and  $[1\bar{1}4]$  and  $[001]$  directions corresponding to  $70.5^\circ$  and  $90^\circ$ , respectively.

In order to study effects related to the crystallography we measured the neutral fraction while rotating the crystal azimuth. These results correspond to measurements mainly in a continuous-beam mode but some cross checks were made using time of flight.

In Fig. 5(b) we show the neutral fraction as a function of the azimuthal angle for different incident energies of Li<sup>+</sup> ions scattering off the surface at a scattering angle of  $83^\circ$  with an exit angle of  $13^\circ$ . A considerable variation with azimuthal angles appears in the  $[1\bar{1}0]$  direction at a grazing exit angle ( $13^\circ$ ). For 0.5-keV incident energy, the neutral fraction increases to  $\sim 10\%$  in the  $[1\bar{1}0]$  direction, which is larger than its value in a random azimuthal orientation by a factor of  $\sim 3.5$ . For 0.6-keV incident energy, the neutral fraction is  $\sim 6.5\%$  in the  $[1\bar{1}0]$  direction. For a 1-keV incident energy, the change is much smaller and a relative variation of 14% of the neutral fraction is observed in the  $[1\bar{1}0]$  direction with respect to a random direction. There is no variation when the incident energy is increased to 2 keV. Results using the TOF technique (not shown) are in qualitative agreement with those obtained using the continuous-beam mode. For Li<sup>+</sup> scattered on a Au(110) surface at a scattering angle of  $135^\circ$  and an exit angle of  $90^\circ$ , no significant dependence of neutral fraction on the azimuthal angle is observed in the energy range investigated.

Figure 6 shows the neutral fraction measured for incident energies from 0.3 to 2 keV for two scattering angles and for a random azimuthal direction. We present data for a scattering angle of  $135^\circ$  (for  $45^\circ$  incidence and normal exit and also for specular scattering) and a scattering angle of  $83^\circ$  for specular reflection. The results corresponding to the scattering angle of  $135^\circ$  are larger than those for the scattering angle of  $83^\circ$  over the incident energy range. The neutral fractions first decrease a little with increasing incident energy and then increase as incident energy increases. Their values vary in the range of  $2\% \sim 15\%$ . The neutral fractions for a given scattering angle depend on the exit angle at large incident energies, but are close to each other at smaller incident energies. Therefore for

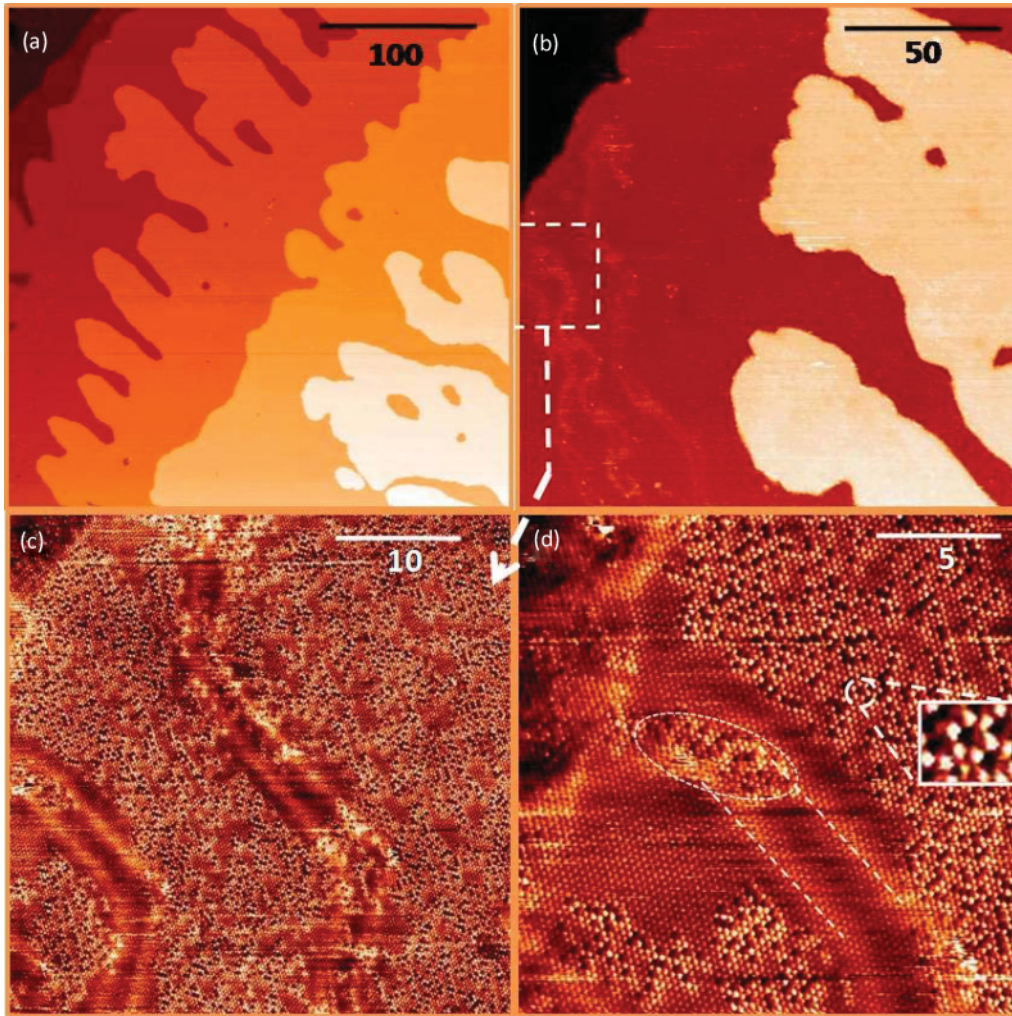


FIG. 4. (Color online) Constant current topographies of the Au(111) surface with  $\sim 2.4$  ML of Ag deposited at room temperature at four different scales: (a)  $320 \times 320$  nm<sup>2</sup>, (b)  $160 \times 160$  nm<sup>2</sup>, (c)  $40 \times 40$  nm<sup>2</sup>, (d)  $20 \times 20$  nm<sup>2</sup>. White dotted straight lines mark the ridges of a pseudo-hcp region.

lower outgoing interaction times, greater neutralization ratios are observed.

In Fig. 7 we show the exit angle dependence for different energies for the  $83^\circ$  scattering angle. A clear increase of the neutral fraction is observed for large exit angles, while a tendency to increase appears at very small exit angles.

### B. Charge transfer processes of Li<sup>+</sup> scattering on a Pd(100) surface

The schematic diagram of the Pd(100) surface is shown Fig. 8(a). The [001] and  $[0\bar{1}1]$  directions correspond to azimuthal angles of  $0^\circ$  and  $45^\circ$ , respectively.

We investigated the neutral fraction as a function of the azimuthal angle for different incident energies of Li<sup>+</sup> ions scattering on Pd(100) surface. This was done by scanning continuously the crystal azimuthal orientation with respect to the ion beam direction. In Fig. 8(b) we show the neutral fraction as a function of the azimuthal angle for 1- and 2-keV energies of Li<sup>+</sup> ions scattering off the surface at a scattering angle of  $83^\circ$  with an exit angle of  $41^\circ$ . In both cases we observe that

the neutral fraction increases when going towards the main channeling ([001]) direction. This increase is greater for the lower incident ion energy.

The increase of the neutral fraction for the main channeling directions for Au(110) and Pd(100) at lower energies suggests that the probability of electron capture when Li<sup>+</sup> stays longer near the surface is larger, similarly to the behavior at low energies and low exit angles.

Figure 9 shows the neutral fraction measured for the Pd(100) surface in conditions similar to the Au(110) surface (see Fig. 6). We present results for scattering angles of  $135^\circ$  (for  $45^\circ$  incidence and normal exit and also for specular scattering) and  $83^\circ$  for specular reflection. The behavior of the neutral fractions is qualitatively similar to the Au(110) case. We again observe that the neutral fractions first tend to decrease with increasing incident energy and then increases as the incident energy increases. Their values are somewhat larger than for Au(110), especially in the low incident energy range.

As for the Au(110) case the exit angle dependence for different energies was measured for the  $83^\circ$  scattering angle (Fig. 10). The neutral fractions tend to increase when going to

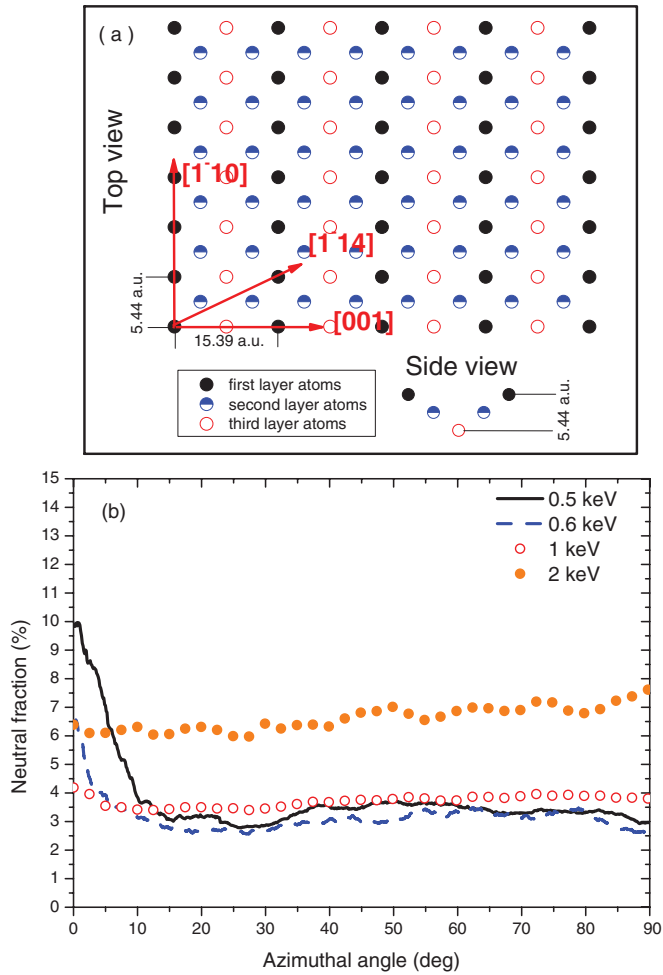


FIG. 5. (Color online) (a) Schematic diagrams of the Au(110) surfaces and the azimuthal angle nomenclature used in the paper. (b) Neutral fractions obtained in scattering on a Au(110) surface as a function of the azimuthal angle for different incident energies of  $\text{Li}^+$ . The results correspond to a scattering angle of  $83^\circ$  and an exit angle of  $13^\circ$ .

small exit angles and a clear increase is observed for large exit angles.

**C. Charge transfer processes of  $\text{Li}^+$  scattering on ultrathin Ag layers on a Au(111) surface**

$\text{Li}^+$  neutralization was studied on Ag layers grown on Au(111). The Ag layer growth was monitored mainly by Li scattering. Scattered Li TOF spectra were acquired for the pristine surface and then as a function of the Ag deposition time. This allows us to check the amount of deposited Ag. In order to minimize sputtering, the incident energy of the beam was chosen to be 0.5 keV and the acquisition time was kept as short as possible.

Figure 11 shows TOF spectra for different amounts of deposited Ag. The scattering angle is  $135^\circ$ , and the incident angle is  $45^\circ$ . When backscattering on Au, Li loses less energy than on Ag. The corresponding elastic energy losses for the given scattering configuration are 57 eV for Au and 99.6 eV for Ag, and positions of the Ag and Au peaks are indicated in the TOF spectrum. Because of this difference the TOF

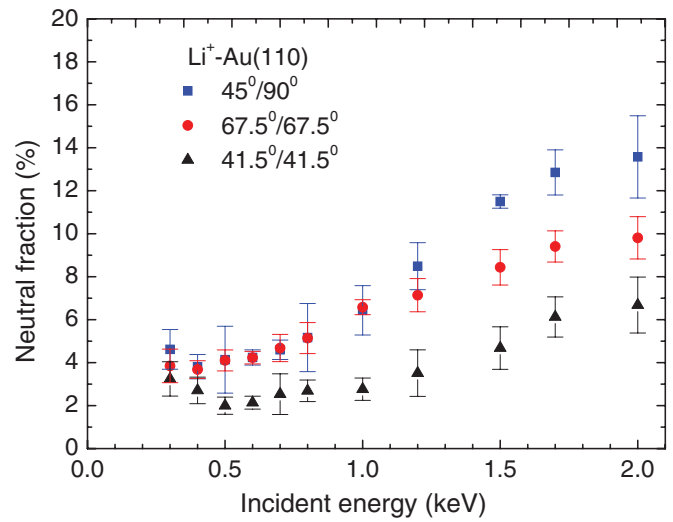


FIG. 6. (Color online)  $\text{Li}^+$  neutral fraction obtained in scattering on a Au(110) surface as a function of incident energy for different scattering geometries and a random scattering azimuth.

spectrum changes and shifts, as shown in Fig. 11. The TOF spectrum shows progressive disappearance of the Au peak. The top TOF spectrum, where gold is essentially not seen is considered to be 1 ML. The small amount of  $\sim 5\%$  of remaining Au at the monolayer stage observed in STM, cannot be discerned unambiguously here. Since the scattering peak on Ag is superposed on that of Au, we chose to measure the ion fraction for 1 ML coverage, when Au is no longer visible. These results are shown in Fig. 12.

We observe that the neutral fraction on the Ag monolayer is found to be very close to the results obtained on a bulk Ag(111) crystal and is much larger than that for Au(111). The neutral fraction of  $\text{Li}^+$  decreases as a function of incident energy and we do not observe an increase at high energies, but rather a plateau seems to be reached.

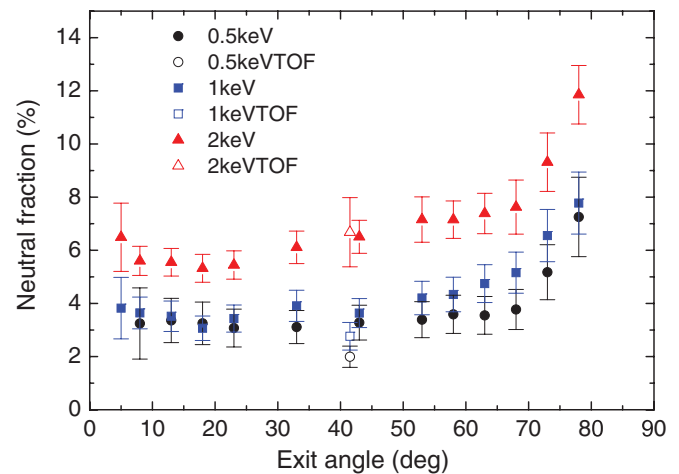


FIG. 7. (Color online) Neutral fraction of  $\text{Li}^+$  on Au(110) as a function of exit angle for the  $83^\circ$  scattering angle. Some points measured by TOF are shown for comparison.

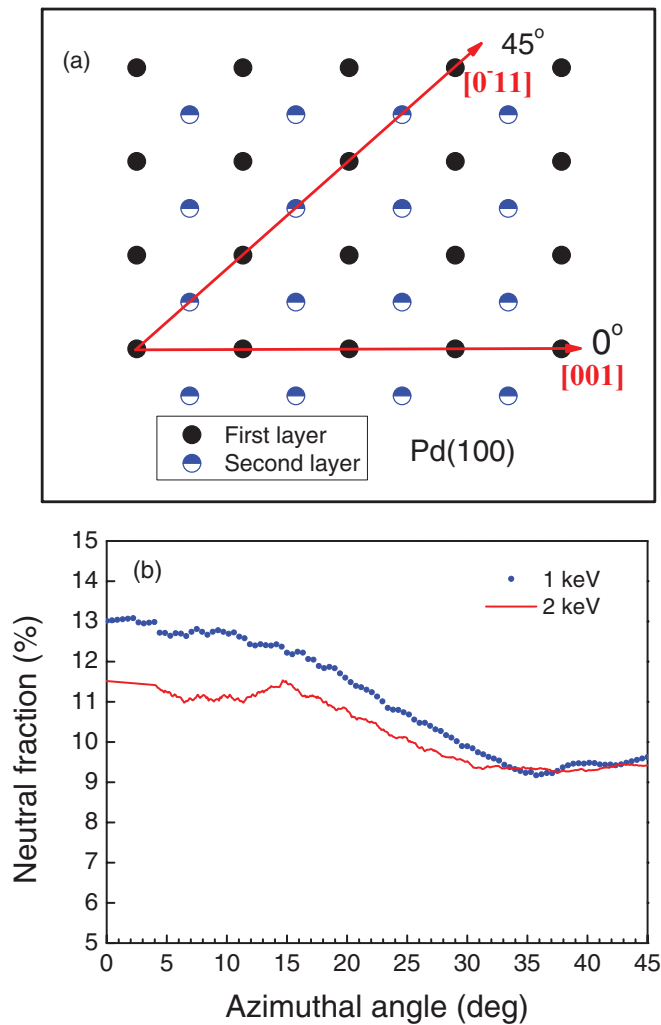


FIG. 8. (Color online) (a) Schematic diagrams of the Pd(100) surfaces and the azimuthal angle nomenclature used in the paper. (b) Neutral fraction for 1- and 2-keV Li<sup>+</sup> ions on Pd(100) surface as a function of the azimuthal angle variation.

## VI. DISCUSSION

In the preceding sections we saw that our results for the large work function surfaces [Pd(100), Au(110)] generally show common characteristics. We see that the neutral fraction tends to first decrease with increasing energy and then increases again. This was also observed by us earlier for the case of Cu(111) and Au(111) [34]. The exit angle dependence is also characterized by a similar trend: decrease of the neutral fraction followed by an increase as the exit angle increases. The case of the Ag layer on Au(111) turns out to be similar to the case of a bulk crystal Ag(111) surface and in the energy range investigated is seen more pronouncedly to decrease with increasing energy and then to flatten out. These findings are somewhat surprising in a “standard” picture of Li neutralization. They also suggest that the basic reasons for the fairly efficient neutralization are the same, in spite of the differences in details of the electronic structure of these surfaces.

In a “standard” picture for neutralization of Li<sup>+</sup> [1], one considers that the Li level is broadened and shifted by the

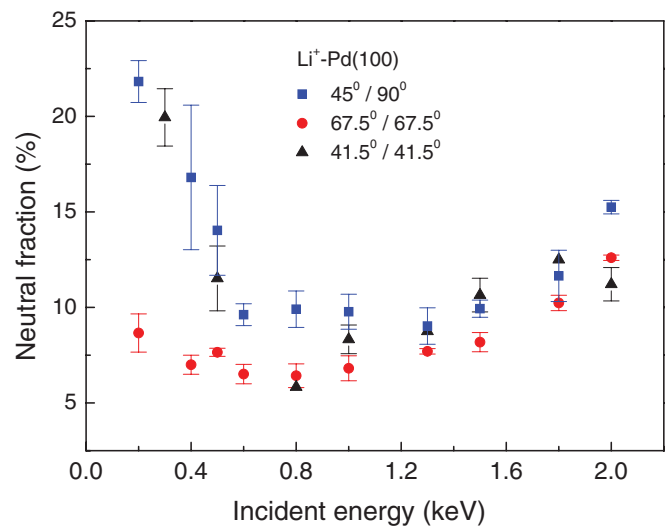


FIG. 9. (Color online) Li<sup>+</sup> neutral fraction for a Pd(100) surface as a function of incident energy for different scattering geometries and a random scattering azimuth.

image potential ( $\delta E = 1/4z$ ) above the Fermi level. Within this picture, ion resonant neutralization occurs at distances where the Li(2s) level remains below the Fermi level and where the interaction is large enough to ensure electron transfer on the collision time scale. Since the work functions of the Au(110) and Au(111) surfaces are larger than 5 eV [32], even for atom-surface distances larger than 8 Å, the Li level always stays above the Fermi level. Therefore, we would not expect significant neutralization for these cases. On the other hand, for Ag(111), with a work function of 4.5 eV, the Li level crosses the Fermi level at a shorter distance of  $\sim 4$  Å allowing neutralization to occur. Moreover, within this picture the neutralization should, due to the lowest interaction time, decrease with increasing incident energy.

As mentioned in the introduction, recent theoretical work [41] indicates that for the Li-Cu system, the Li level shifts below the Fermi level at small Li-surface distances, thus

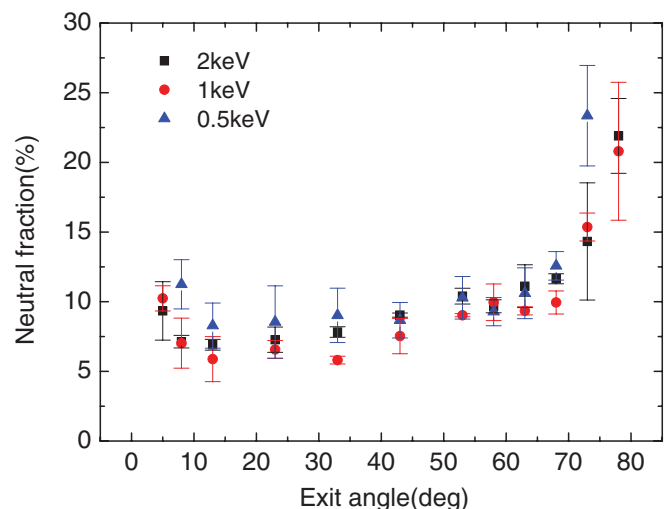


FIG. 10. (Color online) Neutral fraction of Li<sup>+</sup> on Pd (100) as a function of exit angle for the 83° scattering angle.

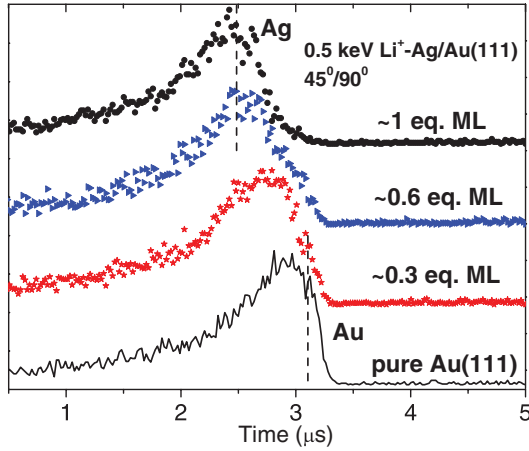


FIG. 11. (Color online) TOF spectra of 0.5-keV  $\text{Li}^+$  scattering on a Au(111) surface as a function of the coverage of Ag layers. The scattering angle is  $135^\circ$ , and the exit angle is along the surface normal. The vertical dash lines mark the position of Au and Ag surface peaks.

resulting in much higher neutralization than expected. These results show the importance of a good description of the Li charge when it is close to the surface. Here we therefore investigated theoretically, using DFT calculations, the behavior of Li in front of the Ag(111), Cu(111), Au(111), and Ag/Au(111) surfaces. In the case of Ag/Au(111) we consider an idealized continuous Ag overlayer.

In Fig. 13, we show the calculated number of lithium valence electrons  $n_{\text{eq}}$  using the Bader charge method for Li on Ag(111), Cu(111), Au(111), and on a Ag monolayer on Au(111), as a function of the atom distance to the outermost top layer. We plot together the calculated Bader charge when Li arrives along the surface normal on the top [ $n_{\text{eq}}^{\text{top}}(z)$ ] and fcc [ $n_{\text{eq}}^{\text{fcc}}(z)$ ] sites, together with an average calculated as

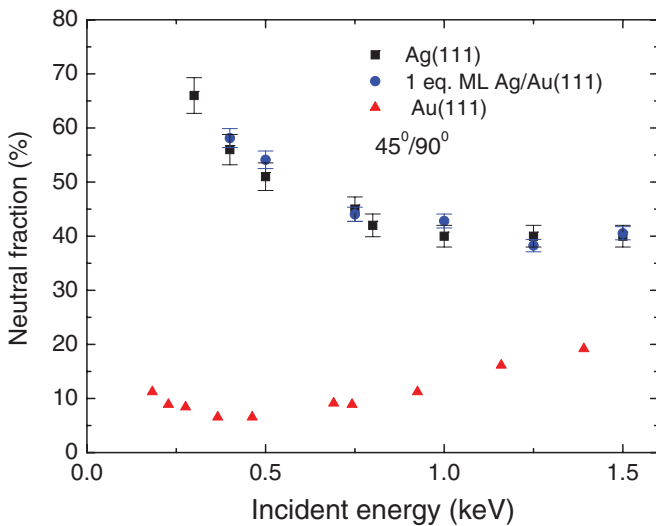


FIG. 12. (Color online)  $\text{Li}^+$  neutral fraction as a function of the incident energy for 1 ML Ag coverage on Au(111), at a scattering angle of  $135^\circ$ , and an exit angle of  $90^\circ$ . For comparison, the experimental data for Ag(111) and Au(111) surfaces are also shown. Data for Au(111) are from Ref. [34].

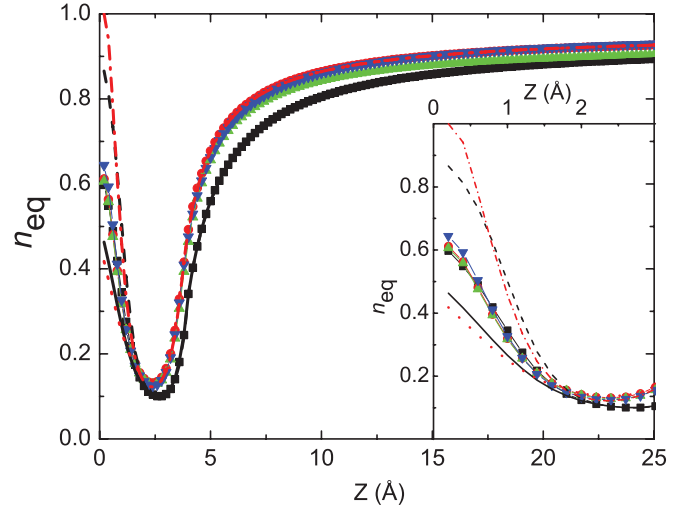


FIG. 13. (Color online) Li number of valence electrons vs distance to the topmost metal layer. Li arriving on the top site  $n_{\text{eq}}^{\text{top}}(Z)$ : dashed line for Au(111) and dash-dot line for Ag(111). Li arriving on the fcc site  $n_{\text{eq}}^{\text{fcc}}(Z)$ : solid line for Au(111) and dotted line for Ag(111). Averaged  $n_{\text{eq}}(z) = 1/3n_{\text{eq}}^{\text{top}}(z) + 2/3n_{\text{eq}}^{\text{fcc}}(z)$ : black squares for Au(111), red circles for Ag(111), green triangles for Ag-Au(111), and blue inverted triangles for Cu(111). The inset shows the details from  $z = 0$  to  $3.17 \text{\AA}$  with enlarged scales.

$n_{\text{eq}}(z) = 2/3[n_{\text{eq}}^{\text{fcc}}(z)] + 1/3[n_{\text{eq}}^{\text{top}}(z)]$ . We can observe that (i)  $n_{\text{eq}}$  has a minimum, slightly dependent on the substrate ( $z_{\text{min}} = 2.646 \text{\AA}$  for Au(111) and  $z_{\text{min}} = 2.434 \text{\AA}$  for the other considered metals) where Li is ionized ( $\text{Li}^+$ ); (ii) for larger distances, the number of valence electrons goes to 1, corresponding to neutral lithium ( $\text{Li}^0$ ) [although the Li charge in front of Au(111) is smaller than in front of the other metal surfaces]; (iii) for smaller distances, the average number of valence electrons increases in a similar way for all surfaces.

This behavior can be explained in terms of the projected density of states (PDOS) on the Li orbitals. In Fig. 14 we show this PDOS calculated for different atom-surface distances of Li on Cu(111). In the bottom panel we add the PDOS on Cu when the Li atom is at  $z = 1.5 \text{\AA}$ . When the atom-surface distance decreases, it can be observed in the Li PDOS how the initially well defined peaks corresponding to  $s$  and  $p$  Li states change their form, due to the hybridization with the Cu  $s$ - $d$  band.

At intermediate distances, the Li atomic states broaden and their energies shift. The  $s$  state goes up and loses electrons and the  $p$  state goes down and takes some electrons. This energy shift has been explained in terms of the image potential model [16–20]. At such distances the atom becomes partially ionized, reaching a minimum of the number of valence electrons at a distance of  $\sim 2.5 \text{\AA}$ . When the atom distance is close enough, due to the hybridization of Li atomic states with the metal states the number of Li valence electrons increases. However, it seems that in this region the description of the static Li charge in terms of position and width of atomic states is no longer valid.

In order to understand the experimental results we must include the time evolution in the system. Assuming a uniform motion along the surface normal  $z = z_0 + v_z t$ , with a constant normal velocity component  $v_z$ , the evolution of the

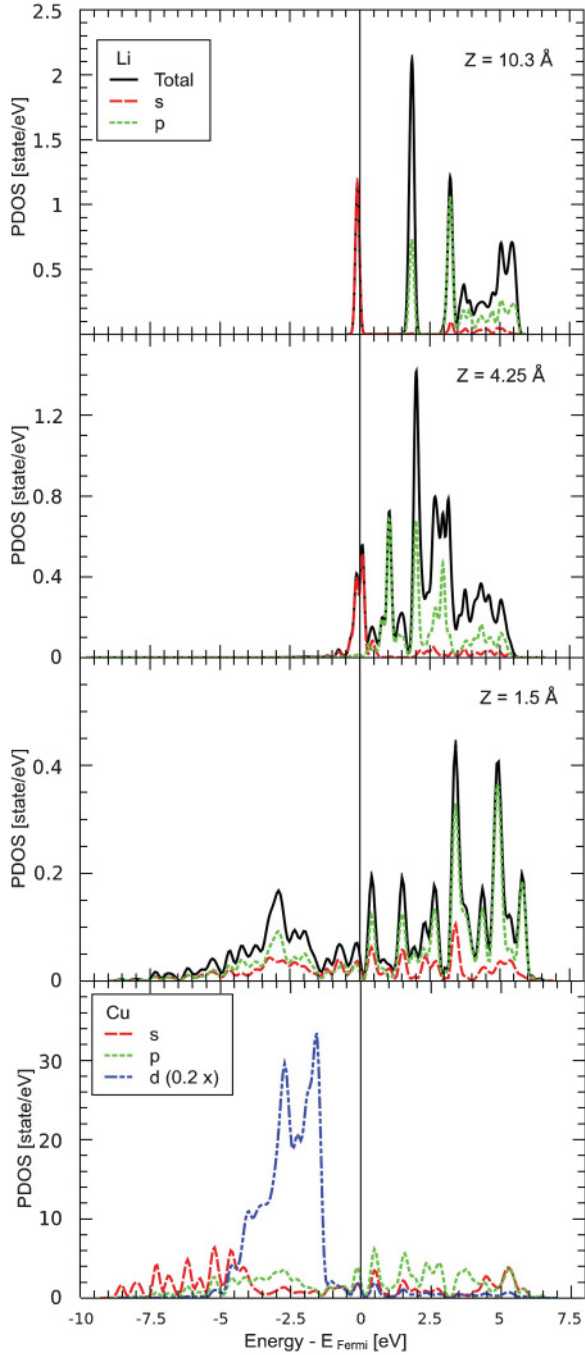


FIG. 14. (Color online) Projected density of states (PDOS) on the Li (three topmost panels) and Cu (bottom panel) orbitals for different atom-surface distances  $z$ . The two bottom panels correspond to the same  $z$ .

number of Li valence electrons can be determined, in a first approximation, from a linearized rate equation [1]:

$$\frac{dn}{dz} = \frac{w(z)}{v_z} [n_{\text{eq}}(z) - n(z)]. \quad (1)$$

Here we only consider the outgoing trajectory [1,2] with normal velocity:

$$v_z = \sqrt{\frac{2E_0}{M_{\text{Li}}}} \sin(\varphi_0),$$

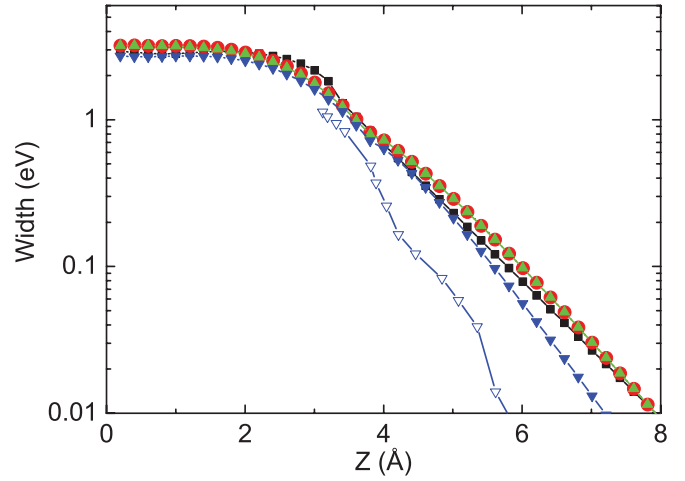


FIG. 15. (Color online) Li width vs distance to the topmost metal layer. Black squares: Au(111); red circles: Ag(111); green triangles: Ag-Au(111); blue filled inverted triangles: Cu(111), blue open inverted triangles: Ref. [41].

where  $E_0$  is the exit energy and  $\varphi_0$  the outgoing angle. The equilibrium number of valence electrons  $n_{\text{eq}}(z)$  corresponds to the calculated value shown in Fig. 13.  $w(z)$  represents the transition probability and is obtained from the width of the calculated projected density of states on the Li atom as a function of the Li-surface distance, which is shown in Fig. 15.

This simplified scheme that links the transition probability with the width of the PDOS on Li does not take into account any dependence on the electron momentum and this introduces an overestimation of the transition probability. Therefore, we define the transition probability by multiplying the obtained width by a free parameter  $\chi$ , which will depend on the particular surface. Finally, solving Eq. (1) the neutral fraction is given by  $n(\infty, E_0)$  and can be written as

$$n(\infty, E_0) = e^{-\int w(z) dz / v_z} \left[ n(z_0) + \int_{z_0}^{\infty} n_{\text{eq}}(z) w(z) \times e^{\int_{z_0}^z w(z') dz' / v_z} dz / v_z \right]. \quad (2)$$

In Fig. 16 we plot the calculated neutral fraction of Li<sup>+</sup> impinging, with an incident angle 45° and an exit angle 90° with respect to the surface plane, on Ag(111) and Ag-Au(111) [Fig. 16(a)], and on Au(111) [Fig. 16(b)], as a function of the exit energy and considering different values of the parameter  $\chi$ . For comparison, we add the experimental data for each case (solid symbols). The distance of closest approach is calculated with the binary collision model from the interaction energy of the dimer Li-metal atom system.

For Ag(111) and Ag/Au(111), the model with a parameter  $\chi$  close to 1 ( $\chi = 0.80$ ) describes reasonably well the experimental energy dependence of the neutralization. The behavior for Ag/Au(111) is very similar to that for Ag(111), as it has been experimentally observed. It is also seen in the figure that the model is able to describe the behavior of the neutralization rate observed in the high-energy region.

For Li<sup>+</sup> impinging on Au(111) the  $\chi$  parameter must be reduced to  $\chi = 0.30$  to be able to reproduce qualitatively the experimental behavior for low and higher energies [see

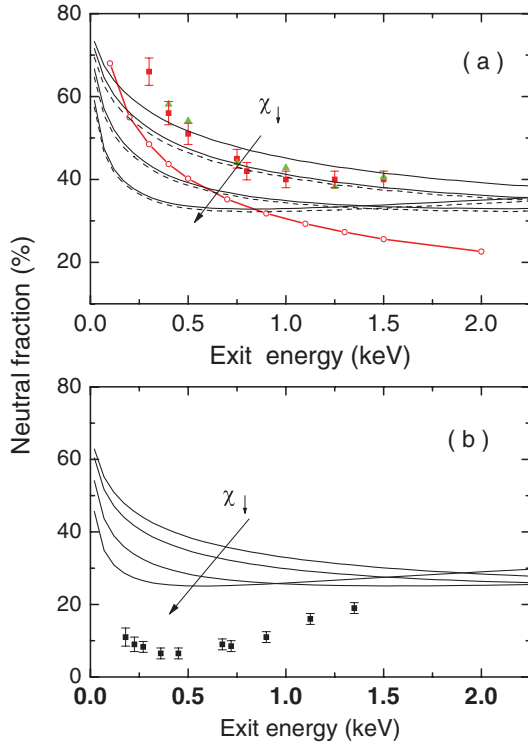


FIG. 16. (Color online) Theoretical neutral fraction for  $\text{Li}^+$  on metals(111) with an incident angle of  $45^\circ$  and an exit angle  $90^\circ$  (with respect to surface plane) for different values of the parameter  $\chi$  (1, 0.8, 0.5, 0.3). Upper panel: solid line: Ag(111) and dashed line: Ag/Au(111); red line with circles: Jellium model. Lower panel: solid line: Au (111). Experimental data: (lower panel) black squares: Au(111); (upper panel) red squares: Ag(111) and green triangles: Ag-Au(111).

Fig. 16(b)]. The decrease of transition probability can be ascribed to the presence of the  $L$  band gap, which is a characteristic of all the (111) faces of noble metals considered here. The differences between Ag on one hand (which needs  $\chi = 0.8$ ) and Au and Cu on the other (with  $\chi = 0.30$ ) comes from the Shockley surface states (SS) that appear in the projected energy gap of the bulk bands. The in-plane dispersion  $E_B(k_{\parallel})$  of these Shockley states can be approximated by a parabola representing a nearly free-electron behavior. The parameters of the parabola, the position of the bottom and its width, are defined by the maximum binding energy and the momentum dispersion of the SS, respectively [56,57]. The lower binding energy of the SS in the case of Ag(111) enables occupied metal states with  $k_{\parallel}$  close to zero to neutralize the Li. On the other hand for Cu(111) and Au(111), the higher binding energy of the SS reduces the availability of occupied metal states for the neutralization. Moreover, the Shockley states are very sensitive to surface modifications such as adsorbates and surface reconstructions. In particularly, a recent experiment [53] led to the conclusion that one monolayer deposition of Ag on a Au(111) reduces the binding energy of the SS, explaining the similar neutralization behavior for Li impinging on Ag(111) and on 1 eq. ML Ag/Au(111). Therefore, the greater value of parameter  $\chi$  in the cases of Ag(111) and Ag/Au(111) could be ascribed to the presence of

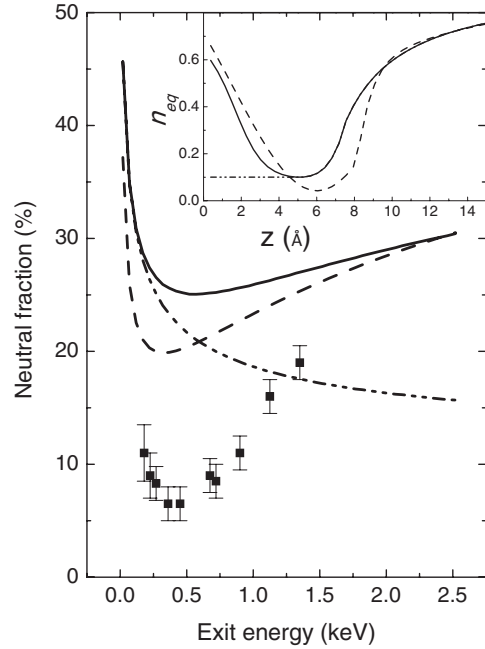


FIG. 17. Neutral fraction for  $\text{Li}^+$  on Au(111) with an incident angle  $45^\circ$  and an exit angle  $90^\circ$  (with respect to the surface plane) for different equilibrium charge models: solid line: Bader; dashed line: PDOS; dash-dot-dot line:  $n = n_{\min}^{\text{Bader}}$  when  $z < z_{\min}$ . Inset: Li number of valence electrons vs distance  $n_{\text{eq}}(z)$  to the topmost metal layer for each model.

available surface states with  $k_{\parallel}$  close to zero near the Fermi level.

The observed overestimation of the neutralization of  $\text{Li}^+$  on Au(111) could be related to the behavior of the equilibrium charge. To evaluate this effect we plot in Fig. 17 the neutralization obtained by considering different models for the equilibrium number of the Li valence electrons. We include the Bader  $n_{\text{eq}}$  (Fig. 13), the  $n_{\text{eq}}$  obtained from the projected density states (PDOS), and the Bader  $n_{\text{eq}}$  with a constant value for  $z < z_{\min}$ . For the PDOS, the minimum of charge decreases and shifts to higher distances. This behavior of the charge in the intermediate distance from the surface results in a decrement for the neutralization at intermediate energies. On the other hand, looking at the neutral fraction obtained considering the Bader  $n_{\text{eq}}$  with a constant value for  $z < z_{\min}$ , it is clear that the neutralization for higher energies is dominated by the increment of the charge close to the surface.

In Fig. 18 we summarize the results for the neutral fraction for  $\text{Li}^+$  impinging on the different surfaces, i.e., Au(111), Ag(111), Ag/Au(111), and Cu(111), comparing the experimental (solid symbols) and theoretical (lines) results. The neutralization behavior as a function of the incident energy can be subdivided into two regimes depending upon perpendicular energy and distance of closest approach.

As may be seen in Fig. 18 at the lowest incidence energies the neutral fractions are high and then decrease when the Li incident energy increases for all metals here considered. We see in Fig. 13 that  $n_{\text{eq}}$  at large distances from the surface is close to unity for all the cases calculated. As energy increases, the final neutral fraction decreases with perpendicular velocity due to lower interaction time, not allowing the establishment of

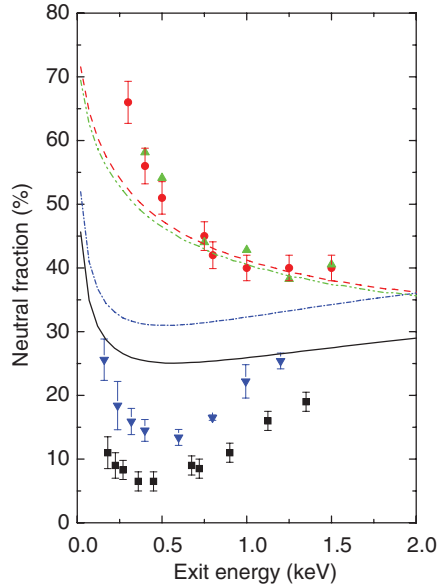


FIG. 18. (Color online) Neutral fraction for Li<sup>+</sup> on (111) faces of metals, incident angle 45° and an exit angle 90°. Theory: dashed line, Ag(111); dash-dot-dot line, Ag/Au(111); short dash-dot line, Cu(111); solid line, Au(111). Solid symbols: black squares: Au( $\chi = 0.3$ ); red circles: Ag(111) ( $\chi = 0.9$ ); green triangles: Ag/Au(111) ( $\chi = 0.9$ ); blue inverted triangles: Cu(111) ( $\chi = 0.3$ ). For Cu(111) the incident angle is 24°. (Cu data from Ref. [34].)

the equilibrium value. The dissimilar behaviors on Au(111), Cu(111), and Ag(111) come from the differences in (i) the transition probabilities, which result in much lower neutral fraction for Cu(111) and Au(111) than for Ag(111); and (ii) the work function, which gives lower equilibrium charge for Au(111) for large Li-surface distances (Fig. 13).

For higher incident energies, what happens close to the surface becomes more important. As can be seen in Figs. 16 and 18 in this energy range, for Ag(111) and Ag/Au(111) the neutral fraction decrease rate is slower than expected by the standard model, and for Au(111) and Cu(111) the neutral fraction begins to increase. This occurs when distances of closest approach are small, corresponding to an increase in the equilibrium charge state (Fig. 13), allowing neutralization near the surface. The picture we have here is then that the incoming incident ion neutralizes near the surface and then a fraction of the neutralized ions survives in the outgoing path. As the outgoing velocity increases, the interaction time for reionization decreases, resulting in the increment of the neutral fraction in our model for high incident energy (Fig. 18), in agreement with experiment. As described before (Fig. 17), if the increase of the equilibrium charge at short distance is not taken into account, the neutral fraction behavior with energy is similar to what is expected in the “standard” model.

In Fig. 19 we show the calculated exit angle dependence of the neutral fraction considering Li<sup>+</sup> exit energies equal to 0.5, 1, and 2 keV for the two models of the number of valence electrons. At the lowest exit angles, when Li stays close to the surface for longer times, the neutralization is efficient so it tends to the adiabatic limit. At high exit angles the neutral fraction also increases for cases when the neutralization was efficient near the surface, because of higher survival due to

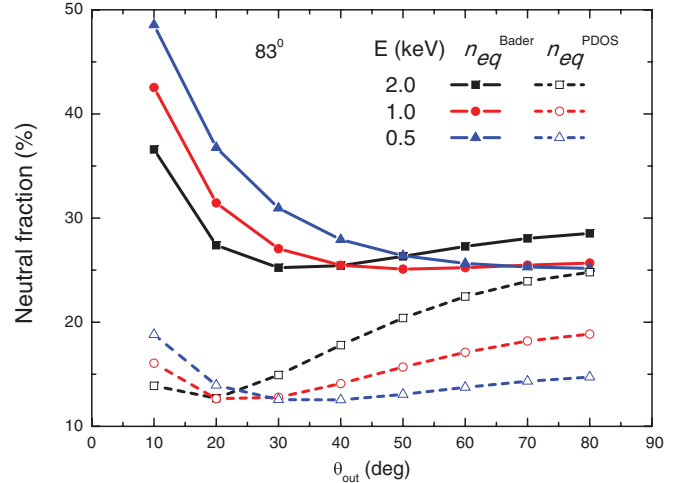


FIG. 19. (Color online) Li<sup>+</sup> neutral fraction dependence on exit angle calculated for the Au(111) case for the scattering angle 83°, using a value of  $\chi = 0.3$ .  $E_{\text{exit}} = 0.5, 1, \text{ and } 2$  keV, and for different determination of  $n_{\text{eq}}$ .

lower interaction times. Qualitatively this is similar to the energy dependence discussed above.

Note that for a complete description, the incoming trajectory, which is not included here when solving the rate equation, should be taken into account and also a better description of the Li-surface potential must be considered to improve the determination of the distance of closest approach.

This analysis of the results allows us to conclude that to understand the increment of Li neutralization for Au(111) and Cu(111), and the behavior for Ag(111) and Ag-Au(111) at high incident energies, it is necessary to take into account the number of Li valence electrons close to the surface. At the lowest energies the increase of the neutral fraction is related to the large  $n_{\text{eq}}$  at large distances that can be reached at low velocities.

To correctly describe the neutralization on Au(111) and Cu(111) we needed to reduce the transition probabilities obtained from the Li state width. This can be explained by the presence of a gap in the projected bulk energy bands, and by the higher binding energy of the surface states compared to the ones in the Ag(111) and Ag/Au(111) surfaces.

In the context of H<sup>-</sup> interactions with metal surfaces an increment in the neutralization has also been observed [58]. In particular, a survival maximum is seen for higher impact velocities which has recently been ascribed to the moving ion’s kinematic influence and associated atomic states energy shift [59]. This process can be important for a fast-approaching ion from the population of empty metal image states by the high kinetic energy electrons released by the ion. If we consider the previously published values of the shifted position of the Li states in front of Cu(111) [18] the excess kinetic energy that should acquire the metal electrons to neutralize the Li via resonance charge transfer when the atomic level shifts up near the surface should be greater than or equal to 3 eV. The ion energy necessary to produce this excess of kinetic energy to the electron from the ion’s normal speed can be calculated considering that  $E_{\text{ion}} \geq 3 \text{ eV} (1836 \text{ Mp})/\sin^2(\theta)$ ,

with  $M_p$  the projectile atomic mass. Then, for Li the ion energy should be  $E_{\text{ion}} \geq 39$  keV. The experimental increment in the neutralization already observed for Li on the coinage metals appears from incident energies close to 1.5 keV. Therefore this model does not seem applicable to explain the behavior studied here.

## VII. CONCLUSIONS

We have presented results of measurements of  $\text{Li}^+$  neutralization on Ag/Au(111), Au(110), and Pd(100) surfaces, which complement our earlier study of neutralization on (111) surfaces of coinage metals [34]. The results for the large work function surfaces (Pd, Au) clearly show some common characteristics: The neutral fraction tends to first decrease with increasing energy and then increase again. This was also observed by us earlier for the case of Cu(111) and Au(111) and is thus quite a general characteristic. The exit angle dependence is also characterized by a similar trend: decrease of the neutral fraction followed by an increase as the exit angle increases.

The case of the Ag layer on Au(111) turns out to be similar to the case of a bulk crystal Ag(111) surface. Compared to the higher work function surfaces, we see a larger neutralization for low energy, a pronounced decrease in the intermediate energy range, and then a plateau.

These findings are somewhat surprising in a “standard” picture of Li neutralization, both in terms of the magnitude of the neutral fractions and the dependence on energy and exit angles. They also suggest that the basic reasons for the fairly efficient neutralization and for the energy and angular characteristics of the fractions are the same, in spite of the differences in details of the electronic structure of these surfaces related to positions of band gaps and surface states.

In order to rationalize these observations we presented a theoretical study of the evolution of the number of Li valence electrons for the (111) surfaces of Ag, Au, and Cu, and for the Ag-covered Au(111) surface, using DFT and a linearized rate equation. Although we treat the temporal evolution within a simple approximation, the study of the static system with *ab initio* calculation helps us to understand the characteristics of the neutralization process.

We show that the increase of Li neutralization for Au(111) and Cu(111), for high incident energies, is mainly determined by the behavior of the number of Li valence electrons close to the surface. This increment is produced by the high hybridization caused by the short-range interactions when Li is close to the surface. The increase of the neutral fraction at low energies is related to the larger number of Li valence electrons at large distances that can be reached at low velocities. These features also allow us to understand the reported behavior of the exit angle dependence.

Although our description is able to describe qualitatively the features of neutralization in  $\text{Li}^+$  scattering, a more complete description is needed to properly take into account the details of the electronic structure in these systems, such as the presence of  $L$  band gaps and surface states of (111) surface of noble metals. Furthermore, an accurate description of the full ion trajectory will be necessary to describe the finer characteristics of this process, in particular the azimuthal dependence of the neutralization process.

## ACKNOWLEDGMENTS

We thank Dr. Hicham Hamoudi for some help in the Ag deposition experiments in Li scattering. Dr. Lin Chen, Jie Shen, and Juanjuan Jia thank the China Scholarship Council which made their stay at ISMO (ex Laboratoire des Collisions Atomiques et Moléculaires) possible.

- 
- [1] J. Los and J. J. C. Geerlings, *Phys. Rep.* **190**, 133 (1990).
  - [2] P. Nordlander and J. C. Tully, *Phys. Rev. B* **42**, 5564 (1990).
  - [3] E. R. Behringer, D. R. Andersson, B. H. Cooper, and J. B. Marston, *Phys. Rev. B* **54**, 14765 (1996).
  - [4] C. A. Keller, C. A. DiRubio, G. A. Kimmel, and B. H. Cooper, *Phys. Rev. Lett.* **75**, 1654 (1995).
  - [5] S. Ustaze, L. Guillemot, V. A. Esaulov, P. Nordlander, and D. C. Langreth, *Surf. Sci.* **415**, L1027 (1998).
  - [6] A. G. Borisov, D. Teillet-Billy, J. P. Gauyacq, H. Winter, and G. Dierkes, *Phys. Rev. B* **54**, 17166 (1996).
  - [7] D. G. Goryunov, A. G. Borisov, G. E. Makhmetov, D. Teillet-Billy, and J. P. Gauyacq, *Surf. Sci.* **401**, 206 (1998).
  - [8] A. G. Borisov, G. E. Makhmetov, D. Teillet-Billy, and J. P. Gauyacq, *Surf. Sci.* **375**, L367 (1997).
  - [9] L. Q. Jiang, Y. D. Li, and B. E. Koel, *Phys. Rev. Lett.* **70**, 2649 (1993).
  - [10] S. Lacombe, L. Guillemot, V. N. Tuan, and V. A. Esaulov, *Nucl. Instrum. Methods Phys. Res. B* **100**, 232 (1995).
  - [11] C. B. Weare and J. A. Yarmoff, *Surf. Sci.* **348**, 359 (1996).
  - [12] S. H. Overbury, *Nucl. Instrum. Methods Phys. Res. B* **27**, 65 (1987).
  - [13] V. A. Esaulov, *Isr. J. Chem.* **45**, 13 (2005).
  - [14] S. H. Overbury, D. R. Mullins, M. T. Paffett, and B. E. Koel, *Surf. Sci.* **254**, 45 (1991).
  - [15] Y. G. Shen, D. J. O’Connor, K. Wandelt, and R. J. MacDonald, *Surf. Sci.* **328**, 21 (1995).
  - [16] Keith Niedfeldt, Emily A. Carter, and Peter Nordlander, *Surf. Sci.* **600**, L291 (2006).
  - [17] A. G. Borisov, J. P. Gauyacq, E. V. Chulkov, V. M. Silkin, and P. M. Echenique, *Phys. Rev. B* **65**, 235434 (2002).
  - [18] A. G. Borisov, A. K. Kazansky, and J. P. Gauyacq, *Phys. Rev. B* **59**, 10935 (1999); *Surf. Sci.* **430**, 165 (1999).
  - [19] T. Hecht, H. Winter, A. G. Borisov, J. P. Gauyacq, and A. K. Kazansky, *Phys. Rev. Lett.* **84**, 2517 (2000).
  - [20] H. Chakraborty, T. Niederhausen, and U. Thumm, *Phys. Rev. A* **69**, 052901 (2004).
  - [21] L. Guillemot and V. A. Esaulov, *Phys. Rev. Lett.* **82**, 4552 (1999).
  - [22] A. R. Canario, A. G. Borisov, J. P. Gauyacq, and V. A. Esaulov, *Phys. Rev. B* **71**, 121401 (2005).
  - [23] K. Niedfeldt, P. Nordlander, and E. A. Carter, *Phys. Rev. B* **74**, 115109 (2006).

- [24] A. R. Canario and V. A. Esaulov, *J. Chem. Phys.* **124**, 224710 (2006).
- [25] G. F. Liu, Z. Sroubek, and J. A. Yarmoff, *Phys. Rev. Lett.* **92**, 216801 (2004).
- [26] M. Wiatrowski, L. Lavagnino, and V. A. Esaulov, *Surf. Sci.* **601**, L39 (2007).
- [27] H. Hövel and I. Barke, *New J. Phys.* **5**, 31 (2003).
- [28] N. Nilius, M. Kulawik, H.-P. Rust, and H.-J. Freund, *Surf. Sci.* **572**, 347 (2004).
- [29] M. Valden, X. Lai, and D. W. Goodman, *Science*, **281**, 1647 (1998).
- [30] I. K. Gainullin, E. Yu. Usman, Y. W. Song, and I. F. Urazgildin, *Vacuum* **72**, 263 (2003).
- [31] E. Y. Usman, I. F. Urazgil'din, A. G. Borisov, and J. P. Gauyacq, *Phys. Rev. B* **64**, 205405 (2001).
- [32] E. V. Chulkov, V. M. Silkin, and P. M. Echenique, *Surf. Sci.* **437**, 330 (1999).
- [33] M. Scheffler and F. Stampfl, in *Handbook of Surface Science*, edited by K. Horn and M. Scheffler (Elsevier, Amsterdam, 2000), Vol. 2, Chap 5, pp. 286–356.
- [34] A. R. Canário, T. Kravchuk, and V. A. Esaulov, *New J. Phys.* **8**, 227 (2006).
- [35] H. Hamoudi, C. Dablemont, and V. A. Esaulov, *Surf. Sci.* **602**, 2486 (2008).
- [36] H. Shao, D. C. Langreth, and P. Nordlander, *Phys. Rev. B* **49**, 13948 (1994).
- [37] D. V. Ledyankin, I. Urazgildin, and V. Yurasova, *Nucl. Instrum. Methods Phys. Res. B* **48**, 585 (1990).
- [38] M. Maazouz, L. Guillemot, and V. A. Esaulov, *Phys. Rev. B* **56**, 9267 (1997).
- [39] M. Maazouz, L. Guillemot, V. A. Esaulov, and D. J. O'Connor, *Surf. Sci.* **398**, 49 (1998).
- [40] B. Obreshkov and U. Thumm, *Phys. Rev. A* **76**, 052902 (2007).
- [41] E. A. García, M. A. Romero, C. González, and E. C. Goldberg, *Surf. Sci.* **603**, 597 (2009).
- [42] U. Heiz and W.-D. Schneider, *J. Phys. D: Appl. Phys.* **33**, R85 (2000).
- [43] A. Bendounan, H. Cercellier, Y. Fagot-Revurat, B. Kierren, V. Yu Yurov, and D. Malterre, *Phys. Rev. B* **67**, 165412 (2003); D. Popović, F. Reinert, S. Hüfner, V. G. Grigoryan, M. Springborg, H. Cercellier, Y. Fagot-Revurat, B. Kierren, and D. Malterre, *ibid.* **72**, 045419 (2005).
- [44] S. R. Kasi, H. Kang, C. S. Sass, and J. W. Rabalais, *Surf. Sci. Rep.* **10**, 1 (1989).
- [45] M. C. Payne, M. P. Teter, D. C. Allen, and J. D. Joannopoulos, *Rev. Mod. Phys.* **64**, 1045 (1992).
- [46] G. Kresse and J. Hafner, *Phys. Rev. B* **47**, 558 (1993).
- [47] G. Kresse and J. Hafner, *Phys. Rev. B* **49**, 14251 (1994).
- [48] P. E. Blöchl, *Phys. Rev. B* **50**, 17953 (1994).
- [49] J. Perdew, K. Burke, and M. Ernzerhof, *Phys. Rev. Lett.* **77**, 3865 (1996).
- [50] H. Monkhorst and D. Pack, *Phys. Rev. B* **13**, 5186 (1976).
- [51] M. Methfessel and A. T. Paxton, *Phys. Rev. B* **40**, 3616 (1989).
- [52] G. Henkelman, A. Arnaldsson, and H. Jónsson, *Comput. Mater. Sci.* **36**, 254 (2006); E. Sanville, S. D. Kenny, R. Smith, and G. Henkelman, *J. Comput. Chem.* **28**, 899 (2007).
- [53] H. Cercellier, C. Didiot, Y. Fagot-Revurat, B. Kierren, L. Moreau, D. Malterre, and F. Reinert, *Phys. Rev. B* **73**, 195413 (2006).
- [54] M. M. Dovek, C. A. Lang, J. Nogami, and C. F. Quate, *Phys. Rev. B* **40**, 11973 (1989).
- [55] T. Miller, A. Samsavar, G. E. Franklin, and T. C. Chiang, *Phys. Rev. Lett.* **61**, 1404 (1988).
- [56] W. Shockley, *Phys. Rev.* **56**, 317 (1939).
- [57] F. Reinert, G. Nicolay, S. Schmidt, D. Ehm, and S. Hüfner, *Phys. Rev. B* **63**, 115415 (2001).
- [58] A. G. Borisov, A. Mertens, S. Wethekam, and H. Winter, *Phys. Rev. A* **68**, 012901 (2003).
- [59] A. Schmitz, J. Shaw, H. S. Chakraborty, and U. Thumm, *Phys. Rev. A* **81**, 042901 (2010).